Spin-disorder state near nonmagnetic impurities in the frustrated antiferromagnet $YMnO_3$

Sumin Lim,[1] Sejun Park,[1] Soonchil Lee,[1,*] Kisoo Park,[2,3] Hasung Sim,[2,3] Je-Geun Park,[2,3] Seongsu Lee,[4] and Helen E. Maynard-Casely[5]

[1]*Department of Physics, KAIST, Daejeon 34141, Republic of Korea*
[2]*Center for Correlated Electron Systems, Institute for Basic Science (IBS), Seoul 08826, Republic of Korea*
[3]*Department of Physics and Astronomy, Seoul National University (SNU), Seoul 08826, Republic of Korea*
[4]*Neutron Science Division, Korea Atomic Energy Research Institute, Daejeon 34057, Republic of Korea*
[5]*Australian Nuclear Science and Technology Organisation, Lucas Heights, New South Wales 2234, Australia*

(Received 6 June 2020; revised 5 November 2020; accepted 9 November 2020; published 24 November 2020)

The effects of nonmagnetic Al impurities on a magnetic bath $YMnO_3$ are studied by magnetization, heat capacity, neutron diffraction, and NMR measurements. Suppression of the Néel order with an increase in the doping rate is evidenced by the heat capacity and M-T curve, also showing vacancy-induced magnetization. Theory predicts that the vacancies in triangular antiferromagnets release the local frustration partially by a readjustment of the spin directions, which results in a net magnetic moment of $0.04S$ around the impurity site, where S is the single spin moment. Interestingly, our NMR results show that the amplitude of the impurity moment is similar to S, which is one order of magnitude larger than a previous prediction. The direction of the impurity moment and neighboring spins generating a hyperfine field at a nonmagnetic impurity site are random. Above T_N, the release of frustration due to a spin-vacancy is evidenced by the enhancement of the antiferromagnetic correlation of spins near impurity sites. Based on careful consideration about the structural distortion, we suggest that this huge spin-disorder originates from the magnetic correlation between impurity moments.

DOI: 10.1103/PhysRevB.102.184427

I. INTRODUCTION

Nonmagnetic impurities in low-dimensional magnets induce various interesting phenomena in the mother material. For instance, nonmagnetic impurity doping in a one-dimensional (1-D) dimerized spin chain system $CuGeO_3$ [1] or the spin ladder $SrCu_2O_3$ [2,3] causes the suppression of the spin gap and an enhancement of the long-range antiferromagnetic order. Regarding YBCO [4–6], a two-dimensional (2-D) square lattice antiferromagnet, nonmagnetic ion doping strongly suppresses the superconductivity and enhances the Néel order. The most interesting aspect of nonmagnetic impurity substitution is that it can produce effective magnetic moments in an antiferromagnetic system.While the properties of magnetic impurities in nonmagnetic bath have been well studied, the microscopic origin of the impurity-induced moment (m_{imp}) due to nonmagnetic impurities in a magnetic bath remains elusive. The effects of these impurities are more complicated in the mother material of a noncollinear, frustrated antiferromagnetic system. The main difference between a collinear and a noncollinear system is the tilting of the nearest-neighboring spins, which induce fractional magnetic moments around the impurity. Frustration, which is the key characteristic of many novel magnetic phases, is also controlled by this impurity doping. The existence of a spin-vacancy in a frustrated system can lead to a new equilibrium point.

$YMnO_3$ is one of the most well-known multiferroic materials. It has ferroelectric ordering of polarization to the c axis at 900 K, and the manganese electron spins form a triangular lattice antiferromagnet [7] on the ab plane. Manganese spins have antiferromagnetic exchange interactions about $J \approx 500$ K, while long-range ordering occurs at 74 K due to the frustration. Neutron-diffraction results confirm that spins have a 120° spin structure and that the ordered moment reaches approximately $3\mu_B$ at 4 K. The electron configuration of Mn^{3+} predicts a spin moment of $4\mu_B$/ion, and one report suggests that this missing moment of $1\mu_B$ is in a quantum fluctuating state [8]. The structural distortion simultaneously occurs at T_N. Several papers report the existence of Mn trimerization, which is induced by 1%–2% of in-plane lattice distortion [9,10]. In addition, impurity doping also affects the lattice structure. Even if doped elements have same valence, still they have different ionic radii compared with the original nuclei and induce chemical pressure in the crystal. There was a report about the effects of Al and Ga doping on the Mn site [11]. These two factors—Mn trimerization and chemical pressure—can deform the crystal structure from the ideal triangular lattice. Thus, careful consideration is required in order to investigate only the effects of magnetic disorder. A study of nonmagnetic Al, Zn, and Ru impurity substitution in $YMnO_3$ by Park *et al.* [12] revealed the suppression of the Néel temperature and an ordered moment in doped materials. However, the microscopic spin structure around impurity sites still remains unknown.

In this paper, we used nuclear magnetic resonance (NMR) to investigate the local spin environment around nonmagnetic

*soonchillee@kaist.ac.kr

Al impurities in $YMnO_3$. From the temperature and angular field dependence of the ^{27}Al NMR spectra, the size and direction of m_{imp} are studied. In the 2-D triangular antiferromagnetic system, a quantum Monte Carlo simulation predicts that the size of the impurity moment due to a spin vacancy is around $0.04S$ [13], where S is the single spin moment. In contrast with the theoretical prediction, our spectral analysis reveals that the amplitude of m_{imp} is similar to the spin moment of the manganese spin S ($\approx 3\mu_B$ in this system) and heads in every direction on the *ab* plane. These results show that substituting a magnetic ion with a nonmagnetic ion in a triangular antiferromagnetic system can be roughly considered akin to adding a single additional spin in a nonmagnetic bath. From the NMR spectra above T_N, we also confirm that nonmagnetic impurities can release the frustration of the spin structure. The local enhancement of antiferromagnetic correlation due to impurity doping shows a spatially inhomogeneous feature. We also estimated the effects of structural distortion due to the impurity doping and concluded that the amount of observed disorder is hard to explain only as a crystalline disorder.

II. EXPERIMENTS

Single crystals of $YMn_{1-x}Al_xO_3$ were grown with a floating zone furnace. The feed rod and seed rod for growth were prepared using Y_2O_3, Mn_2O_3, and Al_2O_3 by a standard solid-state reaction method. All of the starting materials prepared at a stoichiometric ratio were mixed, pelletized, and sintered several times. The final sintering condition was set to 1300 °C for 24 hours, and 4-mm-diameter feed and seed rods with correct compositions were used for the floating zone furnace (Crystal Systems, Japan) growth under ambient conditions with a growth speed was 2 mm/hour. All of our samples were checked to form in the single phase by single-crystal x-ray diffraction (XRD) measurements. Samples were then orientated and cut for several measurements.

The magnetic and thermodynamic properties of the single-crystal samples were characterized from 0.4 to 300 K using a MPMS-XL5 and a PPMS-9ECII (Quantum Design). Neutron-diffraction data of the pure and 10% doped samples were collected on the high-resolution powder diffractometer (HRPD) at the Korea Atomic Energy Research Institute (KAERI). The samples were loaded inside the cryostat and measurements were made at 10 K with a wavelength of $\lambda = 1.835$ Å. A 20% doped sample was measured with the high-intensity powder diffractometer WOMBAT at the Australian Nuclear Science and Technology Organisation (ANSTO) [14]. The samples were placed in a $\lambda = 2.41$ Å neutron beam and patterns were collected in the two-theta (2θ) range of $13.5° \leqslant 2\theta \leqslant 134°$. During the measurements, the samples were cooled to $\approx$4 K, the base temperature of a closed-cycle refrigerator. A crystal structural analysis was done using FULLPROF [15].

The ^{27}Al NMR spectrum was measured from room temperature to liquid helium temperature with an external magnetic field up to seven tesla. The NMR spectra were obtained from the spin-echo signal in our home-built NMR spectrometer. The conventional Hah-echo pulse sequence with a pulse with of 3–5 μs was used. The full spectrum was collected by sweeping the frequency at 0.5 MHz steps. The single-crystal samples are mounted onto the sample stage with careful control of the crystal axis.

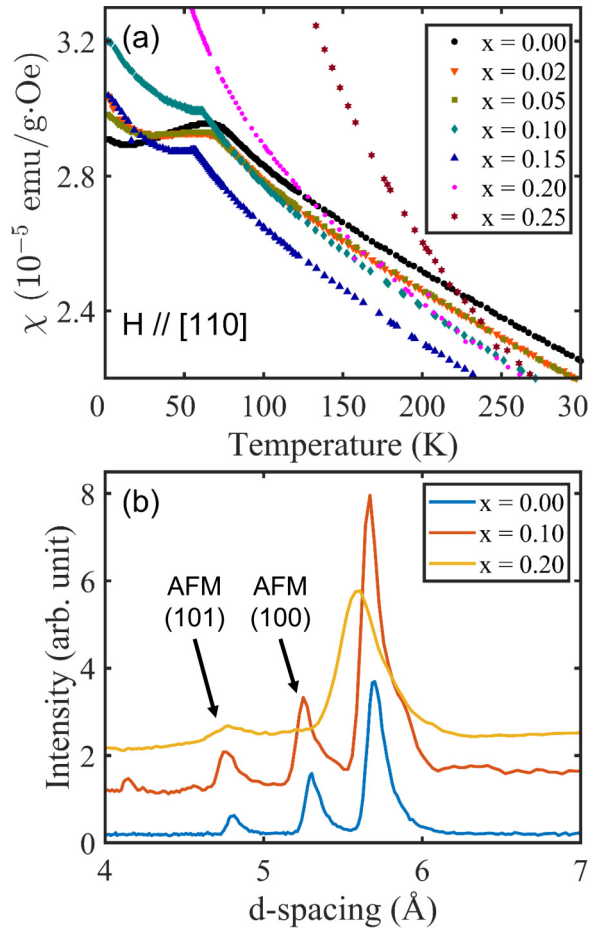

FIG. 1. (a) Susceptibility curves of $YMn_{1-x}Al_xO_3$ samples obtained from 0.4 to 300 K. The external field is applied parallel to the crystal [110] axis. (b) Powder neutron-diffraction data of $YMn_{1-x}Al_xO_3$ samples. The Bragg peaks around 4.8 and 5.2 Å are pure magnetic peaks, which imply 120° spin ordering.

III. RESULTS

In Fig. 1(a) the susceptibility curves of the Al doped $YMnO_3$ samples are presented. The susceptibility of the impurity-doped samples shows an upturn below the Néel temperature T_N, while that of the pure sample shows a monotonic decrease. The anomaly at T_N, which indicates a phase transition, is suppressed as the doping rate is increased. Also, the Curie-Weiss temperatures and Curie coefficients show a linear decrease with increasing doping ratio x, and it guarantees that nonmagnetic impurities are well doped in manganese sites. The heat-capacity measurements also show the same trend, i.e., the suppression of antiferromagnetic ordering. As the doping ratio is increased, amount of susceptibility upturn increases. The samples with impurity ratios exceeding 25% do not show a clear anomaly, which indicates the absence of a Néel temperature. Figure 1(b) shows the neutron-diffraction data of the pure and Al-substituted $YMnO_3$ samples. The pure

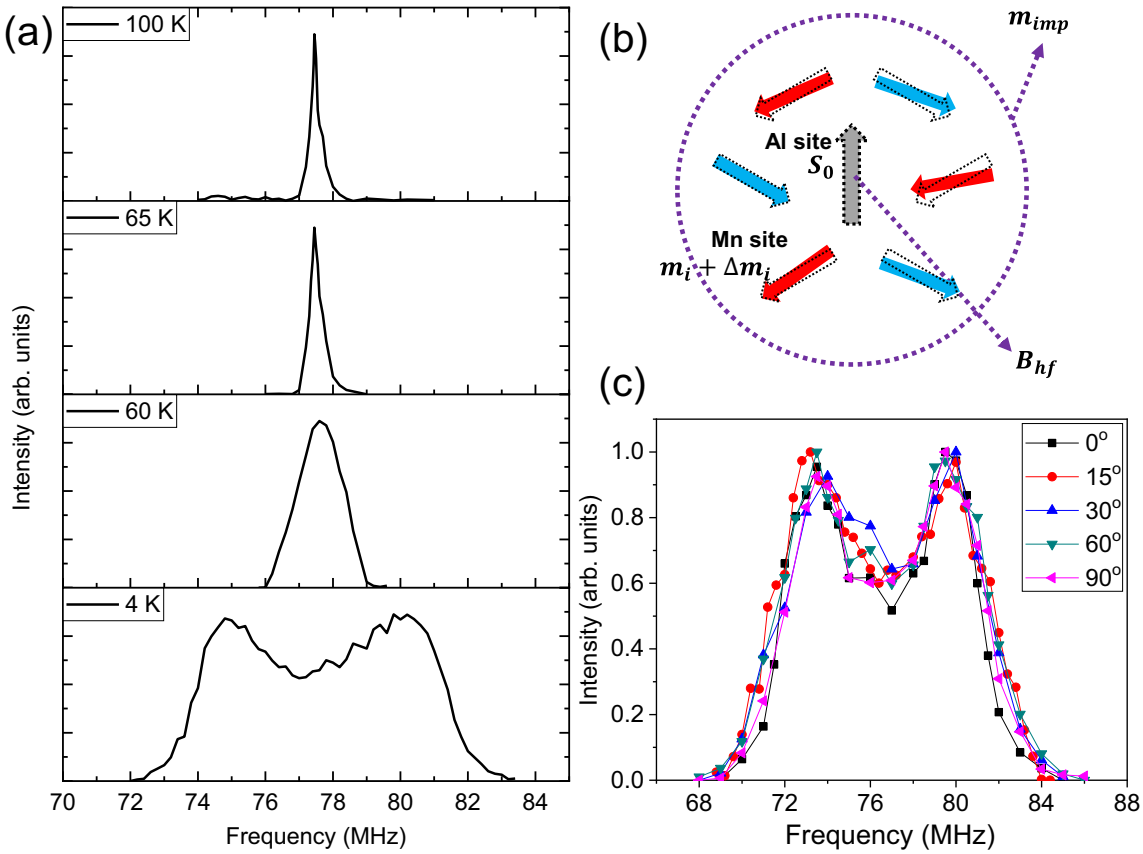

FIG. 2. (a) ^{27}Al NMR spectra of the Al 10% doped sample obtained at temperatures ranging from 100 to 4 K. A 7 T external magnetic field is applied on the axis rotated 35° from the crystal [110] axis to the [001] axis, the angle of which cancels out the nuclear quadrupole broadening. (b) Schematic diagram of spin structure m_{imp} and B_{hf} around an impurity site. (c) ^{27}Al NMR spectra of the Al 5% doped sample obtained at 4 K. The external field is rotated from the [110] crystal axis to the [1$\bar{1}$0] axis. The index is the rotated angle from the [110] axis.

magnetic Bragg peaks around 4.8 Å (101) and 5.2 Å (100) indicates the original 120° spin structure. The ratio of the intensity of these two peaks provides information about the angle between the spin direction and crystal axis. The absence of the (100) Bragg peak and the remaining (101) Bragg peak implies the Γ_4 representation, which means that the crystal (110) axis is parallel to one third of the spins [9]. Therefore, the results in the Al 20% doped sample shows that the 120° spin structure remains. The size of the ordered moment decreases as the doping rate increases. The magnetic moment reduction upon doping is consistent with the susceptibility and heat-capacity measurements. These data indicate that, in a macroscopic view, nonmagnetic impurity doping results in an increase of the magnetic susceptibility. To investigate the microscopic difference between doped and nondoped cases, we measured the Al NMR spectrum of the doped samples.

Figure 2(a) shows the ^{27}Al NMR spectrum of the 10% doped sample obtained at temperatures between 4 and 150 K. An external magnetic field of 7 T is applied to the axis that rotates 35° from [110] to [001] to avoid nuclear quadrupole broadening. The spectrum above the Néel temperature (≈60 K) shows a sharp single peak at the frequency corresponding to the gyromagnetic ratio of the Al nuclei. The linewidth of the spectrum starts to broaden at a temperature below 60 K, finally showing a wide double-peak spectrum at 4 K. This broadening is caused by ordered manganese spins below T_N that generates a hyperfine field at the impurity site. The less-doped samples (2%–5%) show similar spectral linewidth broadening occurring below T_N. The decrease of the external field to 3.5 or 2 T only shifts the center frequency and does not affect the broadening of the linewidth. This results indicates that this broadening is robust against changes in the amplitude of the external field.

Figure 2(b) is a schematic diagram of a 120° spin structure with a nonmagnetic impurity substitution at the center. The six neighboring spins of the substituted site are tilted to reduce the net moment around the impurity. The impurity moment, which is defined as the magnetization difference between two cases when impurity is absent or present, can be written as $m_{imp} = \sum_i \Delta m_i - S_0$, where Δm_i and S_0 are the tilted amount of the six neighbor spin moments and the original spin moment vector of the substituted site, respectively. The manganese spins of nearest-neighboring sites generate a transferred hyperfine field B_{hf} at the impurity site through Mn($3d$)-O($2p$)-Al($2s$, $2p$) orbitals [16]. This hyperfine field can be written as $B_{hf} \propto \sum_i \Delta m_i - 3S_0$, and the detailed derivation is written in Appendix A. Therefore, we can study the local spin structure around impurity sites by investigating the NMR spectrum based on the relationship of $B_{hf} \propto m_{imp} - 2S_0$.

If the size of m_{imp} is two orders of magnitude smaller than S_0, as theory predicts, the following condition will be satisfied:

$B_{hf} \propto m_{imp} - 2S_0 \sim -2S_0$. The NMR spectrum at 4 K plotted in Fig. 2(a) shows that the amount of linewidth broadening is approximately 10 MHz. Considering the gyromagnetic ratio of aluminum, this indicates that the size of the transferred hyperfine field is about ± 0.5 T. The original spin direction S_0 can have six different directions with 60° symmetry [8]. Because the net field is the vector sum of the external field and the internal field, if we apply the external field parallel to the *ab* plane, the nuclear spins of the impurity sites experience six different net fields below T_N. Therefore, a sharp single peak above T_N is expected to split into six peaks below T_N. However, what we actually observe below T_N is a single broad spectrum, as shown in Fig. 2(a). This implies that hyperfine fields at Al nuclear sites have a continuous distribution around ± 0.5 T and not six discrete values. Because B_{hf} is proportional to $m_{imp} - 2S_0$ and the vector $\vec{S}_0$ can only have six discrete directions, this continuous distribution of B_{hf} is the contribution of m_{imp}. It also indicates that the size of m_{imp} has an order similar to that of S_0.

The angle dependence of the NMR spectrum gives us a clearer picture of the spin structure. Figure 2(c) is the NMR spectrum of the Al 5% doped sample obtained at an external field rotated by 0°, 15°, 30°, 60°, and 90° from [110] to $[1\bar{1}0]$. The results show the angle-independence of the NMR spectra, which indicates homogeneity of the B_{hf} distribution in any direction on the *ab* plane. Considering that the S_0 have six discrete directions, this type of angle-independent B_{hf} can only be explained by m_{imp} with the following conditions: (1) a completely random direction and (2) an amplitude about S_0. Therefore, neighboring manganese spins around impurity sites are quite randomly tilted, and this tilting is different for each site.

The Mn trimerization in this material also affects spectral broadening. Although details of lattice distortion differ in each paper [9,10,17–20], they agree that trimerization causes ≈2% of lattice deformation. Because trimerization can change the transferred hyperfine field (B_{hf}) of the system, we considered following two points in our modeling of the hyperfine field mentioned above. First, the definition $m_{imp} = \sum_i \Delta m_i - S_0$ is still valid in this condition. Second, the definition $B_{hf} \propto \sum_i \Delta m_i - 3S_0$ can be changed, because the transferred hyperfine field from the nearest two sites are stronger than those from the other four. The isotropic transferred hyperfine field is an order of magnitude larger than other interactions (anisotropic transferred hyperfine field, direct dipole field) [16], so we only considered isotropic term. Then, we can approximate $B_{hf} \propto \sum_i \Delta m_i - 3S_0 + \alpha(m_1 + \Delta m_1 + m_2 + \Delta m_2)$, where $(1 + \alpha)$ is the enhancement ratio of the transferred hyperfine field due to the trimerization, and m_1 and m_2 are spin moments of two manganese sites of trimer. Because the entire structure is not so deformed from the 120° structure as shown in Fig. 1(b), and sum of m_1 and m_2 is $-S_0$ for any cases, B_{hf} can be rewritten as $\approx \sum_i \Delta m_i - 3S_0 - \alpha S_0$. The size of the transferred hyperfine field as a function of the interatomic distance r is proportional to r^{-6} to r^{-7} [21], and 2% of lattice distortion can maximally generate only 12%–14% enhancement of the field; i.e., an α value of 0.12–0.14. Therefore, Mn trimerization is not the main source of huge impurity moment about S.

The local strain due to the impurity nucleus is also a considerable factor in this system. Previous reports studied deformation of the lattice constant and atomic position in Al- and Ga-doped $YMnO_3$ [11]. Powder and single-crystal XRD results reveal that, in the doping ratio of 2%–10%, change of a lattice constant due to the doping was less than 1%. Also, the deformation of the atom position mainly starts to occur at a doping rate higher than 10%. It indicates that the amount of crystalline disorder due to the local strain of the impurity nucleus is, at least in the doping ratio of 2%–10%, less than the effects of trimerization. Because we concluded that trimerization can maximally induce spin disorder corresponding to impurity moments about $0.12S$ to $0.14S$, the entire disorder in the doped system will not exceed about $0.28S$. Therefore, it is not the main source of the observed impurity moments, which have size about S. We also note that our NMR spectral shape and linewidth of 2%, 5%, and 10% doped samples were almost the same. Because the amount of crystalline disorder increases as the doping ratio increases, this robustness also supports our conclusion.

With regard to m_{imp} around $0.04S$, as the Monte Carlo simulation predicts, the six nearest-neighbor spins have an average angle of ≈110° relative to S_0. The angle distribution of ≈±10° from ≈110° produce the m_{imp} distribution of $\pm S$ (it is easily confirmed that the six nearest-neighbor spins with 120° produce impurity moment of $-S$), and accordingly this is also the case for our sample. In addition, because there is no reason for the six neighboring spins to have an equal amount of tilting, we assume that the actual distribution of the tilting of these spins exceeds ±10°.

The NMR spectra of the Al 2% and 5% doped samples show a similar spectral shape. Also, they are invariant to 90° rotation of the external field. Therefore, at doping ratios of 2%–10%, B_{hf} and m_{imp} have homogeneous distributions in every direction of the *ab* plane.

Figure 3(a) shows the results of a spectrum simulation based on the previous investigation, showing good agreement with the experimental data. The resonance frequency of the NMR spectrum is $f \propto B_{net} = B_{\text{ext}} + B_{hf}$. Under the condition of $B_{\text{ext}} \gg B_{hf}$, B_{net} can be approximated as $B_{\text{ext}} + B_{hf}\cos\theta$, where θ is the angle between B_{ext} and B_{hf}. Additionally, the angle-independent distribution of B_{hf} indicates that the signal intensity of the full spectrum is proportional to the integral of single Gaussian peaks centered at $f = \gamma(B_{\text{ext}} + B_{hf}\cos\theta)$ for all θ : 0–2π. Then, because the frequency f_0 corresponds to $\gamma(B_{\text{ext}} + B_{hf}\cos\theta_0)$, the signal intensity at f_0 is proportional to $1/(d\cos\theta_0/d\theta_0)$.

This type of NMR spectrum displays a typical double-peak shape, as reported in several incommensurate spin spiral [22,23] structures. We used the parameters M and D, which indicate the size of the ordered moment and the amount of spatial inhomogeneity in the spin structure due to the impurity, respectively. In our material, the total linewidth broadening below T_N is directly proportional to B_{hf}. B_{hf} depends on m_{imp} and S_0 and, because both are proportional to the size of the ordered moment, M can be extracted from the temperature dependence of the spectral linewidth broadening. Due to the strong disorder near the impurity, the amplitude of B_{hf} is also different for each site. This size distribution will broaden the single Gaussian peak mentioned above, having convoluted

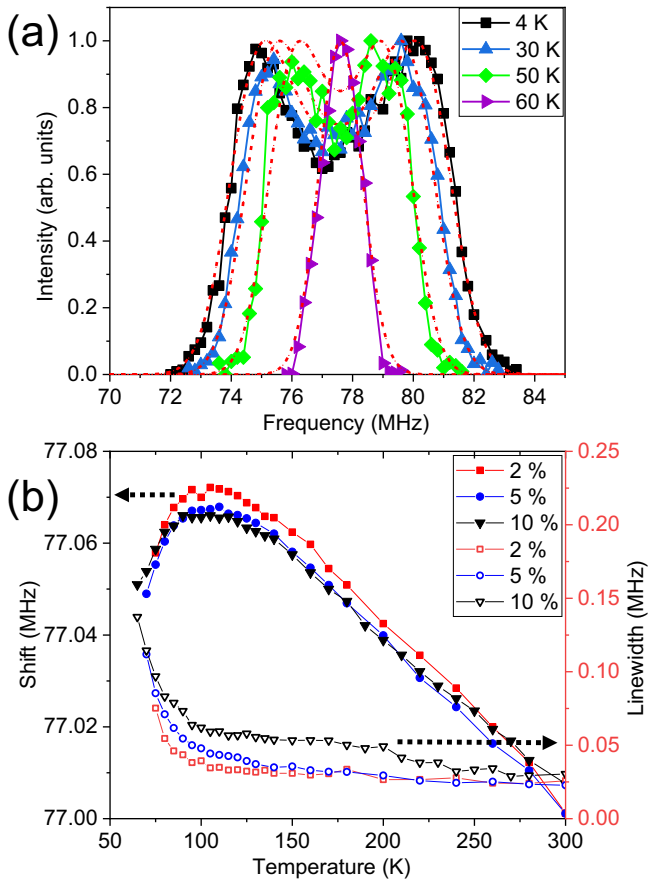

FIG. 3. (a) The observed (solid line) and calculated (red dotted line) NMR spectra of Al 10% doped $YMnO_3$ at a temperature below T_N. See the text for the modeling. (b) The center peak shift (closed symbol) and linewidth (open symbol) of the NMR spectra of a doped sample obtained above T_N.

effects in the full spectrum. The parameter D is extracted from this linewidth of Gaussian peaks. The temperature dependence of the parameter M is consistent with the ordered moment value obtained from neutron-diffraction experiments [10]. This consistency also validates our modeling. The parameter D increases by 50% as temperature decreases from 60 to 4 K. This implies an increase of the spatial inhomogeneity of spin tilting around each impurity site. The spectral intensity and area of the peak on right is higher than those of a peak on left. This asymmetry means that the number of nuclear spins in the condition of B_{hf} parallel to B_{ext} is larger than the number of antiparallel cases. And the angular distribution of B_{hf} is not perfectly homogenous; instead, it is slightly biased toward the B_{ext} direction. Because $B_{hf} \propto m_{imp} - 2S_0$, the distribution of m_{imp} is also slightly biased toward the external field direction. This result is also consistent with the susceptibility upturn in the M-T curve.

The temperature dependencies of the peak shifts (K) and linewidths of the Al NMR spectra of the 2%, 5%, and 10% doped sample obtained above T_N are plotted in Fig. 3(b). The main source of the hyperfine field at the Al site is the transferred hyperfine field from the nearest-neighbor manganese spins. We obtained a coefficient of transferred hyperfine field of 0.18 T/μ_B from the K-χ plot. Considering that Mn ions have magnetic moments of about $3\mu_B$, this result also quite consistent with our spectrum below T_N shows broadening of ≈0.5 T.

Above T_N, in the paramagnetic condition, the size of the transferred hyperfine field is proportional to the local susceptibility of the nearest-neighbor manganese spins. Therefore, the shift and linewidth data in Fig. 3(b) indicate the local susceptibility of the six neighboring manganese spins. The center-peak shift indicates the average susceptibility of six neighboring manganese spins, and the linewidth indicates the inhomogeneity of the susceptibility of each impurities site. All of the 2%, 5%, and 10% samples show an increase in susceptibility with a decrease in temperature until a broad maximum is reached at a temperature of around ≈100 K. This type of susceptibility curve is known to be due to the increase of the short-range antiferromagnetic correlation in the spin system under the condition of $T < J$ without long-range order [24–26].

It is important to note that this broad maximum around 100 K is not observed in the macroscopic susceptibility depicted in Fig. 1(a). The absence of this anomaly in the bulk averaged susceptibility indicates that the increase of the short-range correlation only occurs near the impurity site. Manganese spins far from impurities follow the susceptibility trend of the original $YMnO_3$, which is presented as the bulk susceptibility. Manganese spins near impurities have a dominant effect on the NMR line shift. These data imply that the spin vacancy due to a nonmagnetic impurity locally releases the frustration, resulting in an increase in short-range antiferromagnetic correlation. This increase of the correlation causes a decrease in the local susceptibility. The spectral linewidth in Fig. 3(b) starts to increase at the temperature where the correlation increases. This behavior implies that the amount of the susceptibility decrease due to the correlation enhancement differs for each impurities site. At a temperature in the range of approximately 70–120 K, the spin correlations of impurity NN manganese spins are spatially inhomogeneous.

From the experimental results above, we suggest that there are effective interactions between impurity moments. Below T_N, the amount of spin tilting around an impurity site differs for each site. Above T_N, the linewidth broadening around ≈100 K implies that the enhanced spin correlation around an impurity is also different for each site. These results indicate that there is random disorder in the spin structure. The only randomness in this system is the distance between doped impurities. We quantitatively analyzed the effects of structural distortion in this system, but its amount was expected to be less than 30% of the observed results. Therefore, we suggest that the most plausible source of the disorder is the interaction between spins around the impurity and other impurities. This disorder is observed even in the 2% doped case. Considering that the average distance between impurities is three to four lattice units, the effects of readjustment due to impurity is likely to spread over a same range. This is consistent with the previous reports that the local magnetic-field perturbation due to the impurities on the antiferromagnets spreads several lattice units [27,28]. Also, the impurity-impurity interaction in diluted antiferromagnets are reported to be intrinsic in several theoretical [29,30] and experimental [31] works. And this is

the critical difference between a Monte Carlo simulation and our work in here. The 2%-doping ratio of spin vacancies is large enough to induce spin disorder in entire system.

IV. CONCLUSION

The susceptibility, heat capacity, neutron diffraction, and NMR spectrum are obtained for nonmagnetic Al-doped $YMnO_3$ for a wide temperature range under an external field. Bulk measurements show that nonmagnetic impurities induce effective magnetic moments in the mother material. Evidence of 120° spin structures is still observed even with Al 20% doping in the neutron-diffraction data. The spectral lineshape from ^{27}Al NMR tells us that the amplitude of the impurity moment is similar to S ($3\mu_B$) as a result of the huge disorder in the spin structure near the impurity site. The direction of the impurity moment and the nearest-neighbor spins of the impurities are quite random. Considering the analysis about structural distortion, this disorder is expected to originate from the interaction between impurity moments.

ACKNOWLEDGMENTS

This work was supported by the National Research Foundation of Korea under Contract No. 2019R1F1A1051982. We acknowledge useful discussions with Ki-Hoon Lee, and work at IBS-CCES was supported by IBS-R009-G1.

APPENDIX A: THE RELATIONSHIP BETWEEN THE IMPURITY MOMENT M_{IMP} AND THE HYPERFINE FIELD B_{HF} AT THE IMPURITY SITE IN THIS SYSTEM

Below the temperature T_N, spins around nonmagnetic impurity sites are tilted to reduce the net moment around the sites, and produce impurity moment. In fact, the impurity moment includes the effect from not only the nearest-neighbor (NN) sites but also from the second and third nearest-neighbor sites. However, these contributions are negligible, and we only consider the main term, i.e., the effect of the NN site. The net difference of the moment at a single vacancy site S_0 due to an impurity is expressed as $m_{imp} = \sum_i \Delta m_i - S_0$. These spins of NN sites produce an internal field B_{hf} at the nuclear site of Al. According to a previous experiment [13], three types of transferred fields are possible: (1) an isotropic transferred hyperfine field through Mn($3d$)-O($2p$)-Al($2s$, $3s$), (2) an anisotropic hyperfine field through Mn($3d$)-O($2p$)-Al($2p$), and (3) a direct dipole field from Mn electron spins to the Al nuclear spin. In case (1), the transferred field is directly proportional to the each NN moment, so the net field is the sum of six NN moments. This results in a hyperfine field of $B_{hf,iso} \propto \sum_i \Delta m_i - 3S_0$. In case (2), it produces a dipole-like field at the nuclear site. This means cases (2) and (3) generate fields of the same direction but with different coefficients. The detailed calculation of the dipole field is given below.

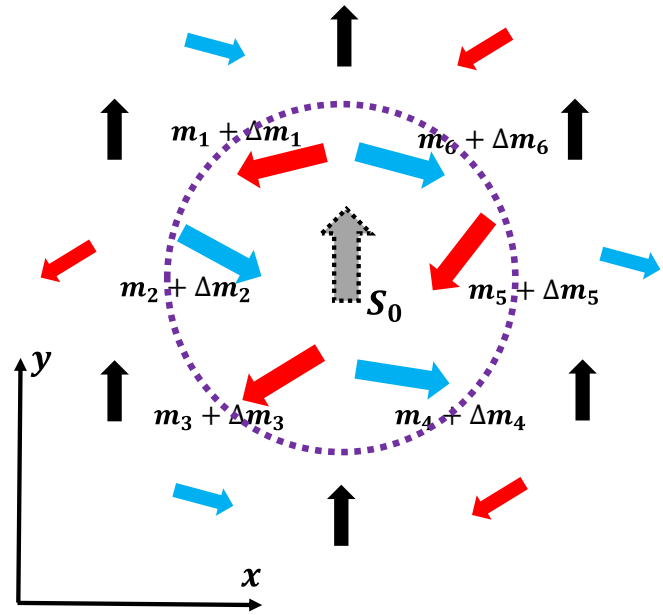

FIG. 4. Schematic diagram of the spin structure around an impurity site. S_0 and $m_i + \Delta m_i$ indicate the spin moment of the substituted site and the readjusted moment of six nearest-neighbor spins, respectively.

As shown in Fig. 4 if we define the direction of S_0 as the y axis, only the y component of the field contributes to the net dipole field due to the symmetry. Therefore, $B_{dip} = B_{dip,y}$. For the same reason, $\sum_i \Delta m_i$ can be written as $\sum_i \Delta m_{i,y}$.

For spin vector m and distance vector r, if we define the unit vector of the direction of r as n (r is the distance between the Mn ion and the Al ion), the dipole field can be written as $\frac{3n(n\cdot m)-m}{4\pi r^3}$. From the six spins of $m_1 + \Delta m_1, m_2 + \Delta m_2, \ldots m_6 + \Delta m_6$, the dipole field at the impurity site is expressed as follows:

$$B_{dip,y} = \frac{\mu_0 m}{4\pi r^3}\left\{ -\frac{3}{2}S_0 - \sum_i \Delta m_{i,y} + 3\left[\frac{3}{4}(\Delta m_{1y} + \Delta m_{3y} + \Delta m_{4y} + \Delta m_{6y}) + \frac{\sqrt{3}}{4}(\Delta m_{6x} + \Delta m_{3x} - \Delta m_{1x} - \Delta m_{4x})\right]\right\}.$$

From the symmetry, the $(\Delta m_{6x} + \Delta m_{3x} - \Delta m_{1x} - \Delta m_{4x})$ term is canceled out. If we assume that the distortions of the six spins are equal, the $(\Delta m_{1y} + \Delta m_{3y} + \Delta m_{4y} + \Delta m_{6y})$ term can be treated as $\frac{2}{3}\sum_i \Delta m_{i,y}$. Therefore, B_{dip} becomes $B_{dip} = \frac{\mu_0 m}{4\pi r^3}(-\frac{3}{2}S_0 + \frac{1}{2}\sum_i \Delta m_i)$. Therefore, the relation $B_{hf,dip}$, $B_{hf,aniso} \propto \sum_i \Delta m_i - 3S_0$ is satisfied. Because three sources of transferred hyperfine field have same form, we can write $B_{hf} = (C_{iso} + C_{aniso} + C_{dipole})(\sum_i \Delta m_i - 3S_0)$, and the coefficients depend on the detailed electronic structure of the site near the impurity.

[1] M. Hase, I. Terasaki, Y. Sasago, K. Uchinokura, and H. Obara, Effects of Substitution of Zn for Cu in the Spin-Peierls Cuprate, $CuGeO_3$: The Suppression of the Spin-Peierls Transition and the Occurrence of a New Spin-Glass State, Phys. Rev. Lett. **71**, 4059 (1993).

[2] M. Azuma, Y. Fujishiro, M. Takano, M. Nohara, and H. Takagi, Switching of the gapped singlet spin-liquid state to an antiferromagnetically ordered state in $Sr(Cu_{1-x}Zn_x)_2O_3$, Phys. Rev. B **55**, R8658 (1997).

[3] N. Fujiwara, H. Yasuoka, Y. Fujishiro, M. Azuma, and M. Takano, NMR Study of Zn Doping Effect in Spin Ladder System $SrCu_2O_3$, Phys. Rev. Lett. **80**, 604 (1998).

[4] M.-H. Julien, T. Fehér, M. Horvatić, C. Berthier, O. N. Bakharev, P. Ségransan, G. Collin, and J.-F. Marucco, ^{63}Cu NMR Evidence for Enhanced Antiferromagnetic Correlations Around Zn Impurities in $YBa_2Cu_3O_{6.7}$, Phys. Rev. Lett. **84**, 3422 (2000).

[5] S. Ouazi, J. Bobroff, H. Alloul, M. Le Tacon, N. Blanchard, G. Collin, M. H. Julien, M. Horvatić, and C. Berthier, Impurity-Induced Local Magnetism and Density of States in the Superconducting State of $YBa_2Cu_3O_7$, Phys. Rev. Lett. **96**, 127005 (2006).

[6] S. Pan, E. W. Hudson, K. Lang, H. Eisaki, S. Uchida, and J. Davis, Imaging the effects of individual zinc impurity atoms on superconductivity in $Bi_2Sr_2CaCu_2O_{8+\delta}$, Nature (London) **403**, 746 (2000).

[7] B. B. Van Aken, T. T. Palstra, A. Filippetti, and N. A. Spaldin, The origin of ferroelectricity in magnetoelectric $YMnO_3$, Nat. Mater. **3**, 164 (2004).

[8] J. Park, J.-G. Park, G. S. Jeon, H.-Y. Choi, C. Lee, W. Jo, R. Bewley, K. A. McEwen, and T. G. Perring, Magnetic ordering and spin-liquid state of $YMnO_3$, Phys. Rev. B **68**, 104426 (2003).

[9] S. Lee, A. Pirogov, M. Kang, K.-H. Jang, M. Yonemura, T. Kamiyama, S.-W. Cheong, F. Gozzo, N. Shin, H. Kimura, *et al.*, Giant magneto-elastic coupling in multiferroic hexagonal manganites, Nature (London) **451**, 805 (2008).

[10] T. Katsufuji, S. Mori, M. Masaki, Y. Moritomo, N. Yamamoto, and H. Takagi, Dielectric and magnetic anomalies and spin frustration in hexagonal $RMnO_3$ (R = Y, Yb, and Lu), Phys. Rev. B **64**, 104419 (2001).

[11] H. Sim, H. Kim, K. Park, M. Lilienblum, M. Fiebig, and J.-G. Park, Doping effects on the ferroelectric transition of multiferroic Y(Mn, Al/Ga)O_3, Phys. Rev. B **98**, 085132 (2018).

[12] J. Park, M. Kang, J. Kim, S. Lee, K.-H. Jang, A. Pirogov, J.-G. Park, C. Lee, S.-H. Park, and H. C. Kim, Doping effects of multiferroic manganites $YMn_{0.9}X_{0.1}O_3$ (X = Al, Ru, and Zn), Phys. Rev. B **79**, 064417 (2009).

[13] A. Wollny, L. Fritz, and M. Vojta, Fractional Impurity Moments in Two-Dimensional Noncollinear Magnets, Phys. Rev. Lett. **107**, 137204 (2011).

[14] A. J. Studer, M. E. Hagen, and T. J. Noakes, Wombat: The high-intensity powder diffractometer at the opal reactor, Phys. B (Amsterdam, Neth.) **385**, 1013 (2006).

[15] J. Rodríguez-Carvajal, Recent advances in magnetic structure determination by neutron powder diffraction, Phys. B (Amsterdam, Neth.) **192**, 55 (1993).

[16] D. Taylor, J. Owen, and B. M. Wanklyn, Hyperfine interactions and electron transfer between metal ions in Fe:$LaAlO_3$ and Cr:$LaAlO_3$, J. Phys. C: Solid State Phys. **6**, 2592 (1973).

[17] P. Brown and T. Chatterji, Neutron diffraction and polarimetric study of the magnetic and crystal structures of $HOMnO_3$ and $YMnO_3$, J. Phys.: Condens. Matter **18**, 10085 (2006).

[18] X. Fabrèges, S. Petit, I. Mirebeau, S. Pailhès, L. Pinsard, A. Forget, M. T. Fernandez-Diaz, and F. Porcher, Spin-Lattice Coupling, Frustration, and Magnetic Order in Multiferroic $RMnO_3$, Phys. Rev. Lett. **103**, 067204 (2009).

[19] A. K. Singh, S. Patnaik, S. D. Kaushik, and V. Siruguri, Dominance of magnetoelastic coupling in multiferroic hexagonal $YMnO_3$, Phys. Rev. B **81**, 184406 (2010).

[20] C. J. Howard, B. J. Campbell, H. T. Stokes, M. A. Carpenter, and R. I. Thomson, Crystal and magnetic structures of hexagonal $YMnO_3$, Acta crystallogr., B Struct. Sci. **69**, 534 (2013).

[21] K. N. Shrivastava, Theory of transferred hyperfine interaction, Phys. Rev. B **20**, 2634 (1979).

[22] A. Zalessky, A. Frolov, T. Khimich, A. Bush, V. Pokatilov, and A. Zvezdin, ^{57}Fe NMR study of spin-modulated magnetic structure in $BiFeO_3$, Europhys. Lett. **50**, 547 (2000).

[23] S. Park, S. Kwon, S. Lee, S. Khim, D. Bhoi, C. B. Park, and K. H. Kim, Interactions in the bond-frustrated helimagnet $ZnCr_2Se_4$ investigated by NMR, Sci. Rep. **9**, 1 (2019).

[24] J.-C. Orain, B. Bernu, P. Mendels, L. Clark, F. H. Aidoudi, P. Lightfoot, R. E. Morris, and F. Bert, Nature of the Spin Liquid Ground State in a Breathing Kagome Compound Studied by NMR and Series Expansion, Phys. Rev. Lett. **118**, 237203 (2017).

[25] M. Fu, T. Imai, T.-H. Han, and Y. S. Lee, Evidence for a gapped spin-liquid ground state in a kagome Heisenberg antiferromagnet, Science **350**, 655 (2015).

[26] P. Mendels, A. Keren, L. Limot, M. Mekata, G. Collin, and M. Horvatić, Ga NMR Study of the Local Susceptibility in Kagomé-Based $SrCr_8Ga_4O_{19}$: Pseudogap and Paramagnetic Defects, Phys. Rev. Lett. **85**, 3496 (2000).

[27] J. Bobroff, H. Alloul, Y. Yoshinari, A. Keren, P. Mendels, N. Blanchard, G. Collin, and J.-F. Marucco, Using Ni Substitution and ^{17}O NMR to Probe the Susceptibility $\chi(q)$ in Cuprates, Phys. Rev. Lett. **79**, 2117 (1997).

[28] S. Ouazi, J. Bobroff, H. Alloul, and W. A. MacFarlane, Correlation length in cuprate superconductors deduced from impurity-induced magnetization, Phys. Rev. B **70**, 104515 (2004).

[29] A. Sen, K. Damle, and R. Moessner, Fractional Spin Textures in the Frustrated Magnet $SrCr_{9p}Ga_{12-9p}O_{19}$, Phys. Rev. Lett. **106**, 127203 (2011).

[30] A. Sen and R. Moessner, Topological Spin Glass in Diluted Spin Ice, Phys. Rev. Lett. **114**, 247207 (2015).

[31] A. D. LaForge, S. H. Pulido, R. J. Cava, B. C. Chan, and A. P. Ramirez, Quasispin Glass in a Geometrically Frustrated Magnet, Phys. Rev. Lett. **110**, 017203 (2013).